Proceedings World Geothermal Congress 2020+1
Reykjavik, Iceland, April - October 2021

Temperature Transient Tests: Modeling, Interpretation, and Nonlinear Parameter Estimation

Davut Erdem Bircan and Mustafa Onur

[+]McDougall School of Petroleum Engineering Stephen, The University of Tulsa, 800 South Tucker Drive, Tulsa OK 74104

dab6565@utulsa.edu and mustafa-onur@utulsa.edu

Keywords: Temperature transient data, Analytical Modeling, Interpretation, Nonlinear Parameter Estimation

ABSTRACT

This study presents semi-analytical and analytical solutions based on a coupled transient wellbore/reservoir thermal model to predict temperature transient measurements made under constant rate and bottom-hole pressure production as well as variable rate and bottom-hole pressure production histories in a vertical or an inclined wellbore across from the producing horizon or at a gauge depth above it. Slightly compressible, single-phase, and homogeneous infinite-acting single-layer geothermal reservoir system is considered. The models account for Joule-Thomson heating/cooling, adiabatic fluid expansion, conduction and convection effects both in the reservoir and wellbore. The transient wellbore model accounts for friction and gravity effects. The solutions of the analytical and semi-analytical reservoir models are verified by use of a general-purpose thermal simulator. Wellbore temperatures at a certain gauge depth are evaluated through a wellbore thermal energy equation coupling the reservoir temperature equation. It is shown that unlike the "sandface" temperature measurements made close to the producing zone, the temperature measurements made at locations significantly above the producing horizon are dependent upon the geothermal gradient and radial heat losses from the wellbore fluid to the formation on the way to gauge and hence more difficult to interpret for well productivity evaluation and reservoir characterization. The solutions can be used as forward models for estimating the parameters of interest by nonlinear regression built on a gradient-based maximum likelihood estimation (MLE) method. A methodology, based on straight line analyses of flow regimes (as derived from analytical solutions) identified on log-log diagnostic plots of sandface and wellbore temperature-derivative data, is proposed to obtain good initial guesses of parameters which derive the MLE objective function to have reliable optimized estimates.

1. INTRODUCTION

The reservoir characterization through integration of dynamic data such as pressure, rate, etc., through history matching has become commonplace throughout the petroleum and geothermal industries. Although temperature data are routinely recorded in well test applications, the use of temperature data for estimating the parameters controlling the fluid and heat flow for the purpose of reservoir characterization has often been ignored in the past. The temperature data for history matching has recently attracted the attention of various researchers. In the petroleum and geothermal literature, it has been shown that temperature in addition to pressure can be a good source of data for reservoir characterization by the use of simple both lumped-parameter and distributed-parameter (1D, 2D and 3D) flow models (Duru and Horne 2010, 2011a,b; Sui et al. 2008a,b; Palabiyik et al. 2013, 2015, 2016; Sidorova et al. 2015; Onur et al. 2016, 2017; Mao and Zeidouni 2018).

Earlier works on transient sandface temperature behaviors trace back to Chekalyuk (1965). Decoupling the pressure diffusivity equation and the thermal energy balance equation, Chekalyuk (1965) was the first to present an analytical temperature solution for constant-rate drawdown tests (with no skin effects) for single-phase flow of slightly compressible fluid. His solution for the thermal energy balance equation was obtained by using the well-known Boltzman transformation for a line-sink well. Here and throughout in this paper, a line-sink well is referred to a production well having a vanishingly small radius. Using the same assumptions of Chekalyuk (1965), Ramazanov and Nagimov (2007) used the method of characteristics to predict sandface temperatures for single-phase flow of slightly compressible fluid in homogeneous reservoir. Later, in a series of papers, Duru and Horne (2010, 2011a, 2011b) used a non-isothermal model which also decouples the pressure diffusivity and the thermal energy balance equations. Using this method, Duru and Horne (2010) proposed a model to predict sandface temperatures for variable surface rate problems with no wellbore storage and skin. Chevarunotai et al. (2018) proposed an analytical solution for estimating the flowing-fluid temperature distribution in a single-phase homogeneous oil reservoir with constant rate production, including the J-T effect and heat transfer to overburden and under-burden strata. However, their solution does not consider the skin effect. Onur and Cinar (2017a) gave an analytical solution of temperature in homogeneous reservoirs, solving the thermal energy equation using the Boltzmann transformation, for both drawdown and buildup considering a slightly compressible fluid in homogeneous reservoirs. They also provided a temperature solution that includes the effect of skin as an infinitesimally thin zone adjacent to the wellbore. Then they presented a methodology for performing semilog-straight lines analysis on temperature data jointly with pressure data. Then Onur et al. (2017) presented a coupled reservoir/wellbore semi-analytical solution to predict temperature transient along the wellbore in presence of skin. They included the effects of wellbore storage and momentum to model the heat loss along the wellbore in their solution. Galvao (2018) and Galvao et al. (2019) presented a coupled wellbore/reservoir thermal analytical model which provides accurate transient temperature flow profiles along the wellbore, accounting for heat losses to strata and fluid density variation. Panini et al. (2019) presented an approximate analytical solution for predicting drawdown temperature transient behaviors of a fully penetrating vertical well in a two-zone radial composite reservoir system. They used their analytical solution as a forward model for estimating the parameters of interest by nonlinear regression built on a gradient-based maximum likelihood estimation (MLE) method. Their results show that the rock, fluid and thermal properties of the skin zone and non-skin zone can be reliably estimated by regressing on temperature transient data jointly with pressure transient data in the presence of noise. Onur and Ozdogan (2019) very recently presented semi-analytical solutions to investigate the temperature transient behavior of a vertical well producing slightly compressible fluid (oil and water system) under specified constant-bottom-hole pressure or rate in a no-flow radial composite

reservoir system and presents graphical analysis procedures for analyzing such temperature transient data jointly with pressure or rate transient data.

Most of the works cited in the previous paragraph considered oil reservoirs. The works considering modeling and interpretation of sandface temperature transient data for liquid-dominated geothermal reservoir were also presented; for instance, see Palabiyik et al. (2013, 2015, 2016), Onur and Palabiyik (2015), and Onur et al. (2016). In this paper, we extend the works of Panini et al. (2019), Onur and Ozdogan (2019) and Galvao (2018) and Galvao et al. (2019) to liquid-dominated geothermal reservoirs.

The paper is organized as follows; First, we present mathematical model and assumptions used to derive analytical and semi-analytical solutions for predicting sandface transient temperatures and wellbore temperatures. Here, wellbore temperatures refer to temperatures measured inside the wellbore at a certain gauge location above the producing horizon. Then, we verify the analytical and semi-analytical solutions by using CMG STARS (2006). Finally, we present nonlinear regression analysis of temperature transient data with or without with pressure transient data for estimating formation parameters by using the maximum likelihood estimation (MLE) method.

2. PHYSICAL SYSTEM, MATHEMATICAL MODEL AND ASSUMPTIONS

As in Palabiyik et al. (2016), we consider non-isothermal flow of single-phase liquid-water (also called as liquid-dominated) in confined geothermal reservoirs. The reservoir pressure (p) and temperature (T) conditions of a single-phase liquid geothermal reservoir can lie in between 0.5 MPa and 50 MPa for p and between 303.15 K (30 °C) and 573.15 K (300 °C) for T. So, the single-phase region considered in this study covers a wide range of reservoir pressure and temperature conditions which may be encountered for single-phase liquid-water geothermal reservoirs (see Fig. 1), and the single-phase liquid region of the phase envelope where the J-T coefficient (denoted by ε_{JTw} in K/Pa) can take negative or positive values, as can be seen from Fig. 2 depending on p and T values. For instance, ε_{JTw} becomes positive in the single-phase liquid-water case if $T > 525$ K (251.85 °C) and $p \geq 10$ MPa. If ε_{JTw} is negative, fluid heats up with pressure drop, while fluid cools down with pressure drop if ε_{JTw} is positive. If $\varepsilon_{JTw} = 0$, no J-T heating or cooling is expected. Hence, one should expect the J-T heating or cooling effect of reservoir fluid depending on the initial conditions of reservoir pressure and temperature during drawdown and buildup tests.

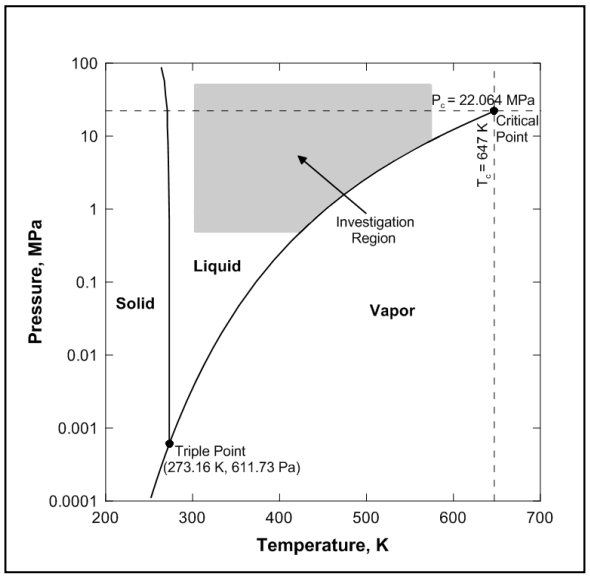

Fig. 1: p-T phase diagram for water (after Palabiyik et al. 2016)

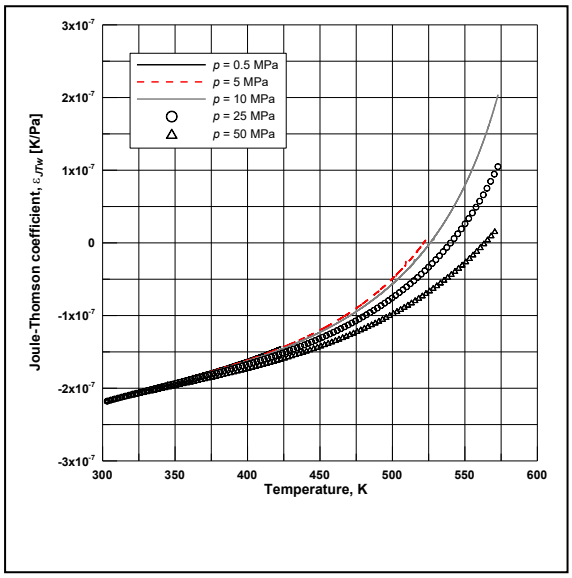

Fig. 2: J-T coefficient as a function of p and T for water (after Palabiyik et al. 2016)

The mathematical model for the reservoir is based on the following basic assumptions:

- flow is single-phase liquid-water without discontinuous gas phase in the reservoir so that water saturation is hundred percent,
- the fluid flow is governed by Darcy's law and is 1D radial towards a vertical well open to flow through the entire reservoir thickness,
- reservoir is radially composite, where each zone is homogeneous and isotropic. The inner zone represents the skin zone for $r_w < r < r_S$, and the outer zone represents the infinite extended reservoir, from $r = r_S$ to infinity (see Fig. 3). In equations to be given later, the skin zone properties are designated by the subscript S, whereas the outer (nonskin zone) properties are designated by the subscript O. Note that the outer zone is actually a water zone,
- the solid matrix is rigid so that it has zero velocity,
- the solid matrix and the liquid water are in thermal equilibrium in order that their temperatures are identical, i.e., $T_s = T_w = T$,
- there exists no heat transfer to over- and under-burden strata from the reservoir, and
- the effective thermal conductivity of rock is homogeneous, isotropic and independent of pressure and temperature.

As to the wellbore model shown in Fig. 3, we consider that the production occurs in a cased vertical wellbore through a fully perforated pay zone where the top of the producing zone in the vertical direction is at $z = 0$, and the wellhead is at $z = L_w$, where L_w represents the total length of the wellbore from the top of the reservoir. Our wellbore model to be presented is quite general in that one can consider any inclination angle of the wellbore. Throughout, we use the International System of Units (SI) for presenting our model equations.

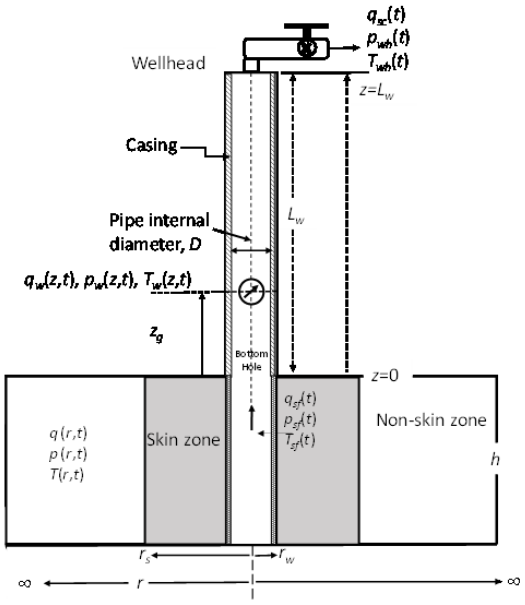

Figure 3: Schematic of a coupled nonisothermal wellbore and reservoir system (after Onur et al. 2017b).

2.1 Reservoir Temperature Equation

As derived by Palabiyik et al. (2016) and Cinar and Onur (2017a) with the previously stated assumptions, the partial differential equation describing spatial and temporal changes of temperature distribution can be given as:

$$\frac{\partial T}{\partial t} + u_c(r,t)\frac{\partial T}{\partial r} - \frac{1}{r}\frac{\partial}{\partial r}\left(r\alpha_t(r)\frac{\partial T}{\partial r}\right) = \varphi_t^*(r)\frac{\partial p}{\partial t} + \varepsilon_{JTw}(r)u_c(r,t)\frac{\partial p}{\partial r}. \tag{1}$$

In Eq. 1, u_c is referred to as the velocity of convective heat transfer, defined by

$$u_c(r,t) = c_{pR}(r)v_r = -c_{pR}\kappa(r)\frac{\partial p}{\partial r}, \tag{2}$$

where c_{pR} is the ratio of volumetric heat capacity of flowing fluid phase to the volumetric heat capacity of the fluid-saturated rock, given by

$$c_{pR}(r) = \begin{cases} c_{SpR} = \dfrac{\rho_S c_{pS}}{(\rho c_p)_{St}} & \text{if } r_{wb} < r < r_S \\ c_{OpR} = \dfrac{\rho_w c_{pw}}{(\rho c_p)_{Ot}} & \text{if } r_S < r < \infty \end{cases} \tag{3}$$

and (ρc_p) is referred to as the volumetric heat capacity of the water-saturated rock, defined by

$$(\rho c_p)_t = \begin{cases} (\rho c_p)_{St} = \phi_S(\rho_w c_{pw})_S + (1-\phi_S)(\rho_s c_{ps})_S & \text{if } r_{wb} < r < r_S \\ (\rho c_p)_{Ot} = \phi_O(\rho_w c_{pw})_O + (1-\phi_S)(\rho_s c_{ps})_O & \text{if } r_S < r < \infty \end{cases} \tag{4}$$

and κ is the mobility function defined by:

$$\kappa(r) = \begin{cases} \kappa_S = \left(\dfrac{k}{\mu}\right)_S & if \;\; r_{wb} < r < r_S \\ \kappa_O = \left(\dfrac{k}{\mu}\right)_w & if \;\; r_S < r < \infty \end{cases}. \tag{5}$$

In Eq. 1, α_t, φ_t^*, and ε_{JTw} represent the thermal diffusivity and the effective adiabatic-expansion coefficient of the water-saturated porous medium, and the J-T coefficient of fluid, respectively, defined by

$$\alpha_t(r) = \begin{cases} \alpha_{St} = \dfrac{\lambda_{St}}{(\rho c_p)_{St}} & \text{if } r_{wb} < r < r_S \\ \alpha_{Ot} = \dfrac{\lambda_{Ot}}{(\rho c_p)_{Ot}} & \text{if } r_S < r < \infty \end{cases}, \tag{6}$$

where λ_{St} and λ_{Ot} are the thermal conductivity of the saturated porous medium in the skin and non-skin zone, respectively,

$$\varphi_t^*(r) = \begin{cases} \varphi_{St}^* = \dfrac{(\rho c_p \varphi)_{St}}{(\rho c_p)_{St}} & \text{if } r_{wb} < r < r_S \\ \varphi_{Ot}^* = \dfrac{(\rho c_p \varphi)_{Ot}}{(\rho c_p)_{Ot}} & \text{if } r_S < r < \infty \end{cases} \tag{7}$$

where $(\rho c_p \varphi)$ is referred to as the adiabatic-expansion coefficient of the water, defined by

$$(\rho c_p \varphi)_t(r) = \begin{cases} (\rho c_p \varphi)_{St} = \phi_S (\rho_w c_{pw} \varphi_w)_S & \text{if } r_{wb} < r < r_S \\ (\rho c_p \varphi)_{Ot} = \phi_O (\rho_w c_{pw} \varphi_w)_O & \text{if } r_S < r < \infty \end{cases} \tag{8}$$

where φ_w is the adiabatic expansion coefficient of water and it is related to the flowing phase J-T coefficient of water by the following relationship (Moore, 1983),

$$\varphi_w = \varepsilon_{JTw} + \frac{1}{\rho_w c_{pw}} \tag{9}$$

and

$$\varepsilon_{JT}(r) = \begin{cases} \varepsilon_{JTS} & \text{if } r_{wb} < r < r_S \\ \varepsilon_{JTO} & \text{if } r_S < r < \infty \end{cases} \tag{10}$$

In Eqs. 1-9, $c_{pw,}$ and φ_w represent the isobaric specific heat capacity and the adiabatic-thermal expansion of water, respectively, and ε_{JTS} and $\varepsilon_{JTO} (= \varepsilon_{JTw})$ represent the J-T coefficient for the skin zone fluid and outer zone fluid (water), respectively. In our applications, although not necessary, we will assume that the J-T coefficients, viscosities and thermal rock and fluid properties are identical for both the skin zone and the non-skin zone.

We use following initial, inner and outer boundary conditions, respectively for the temperature equation given by Eq. 1:

$$T(r, t = 0) = T_i, \tag{11}$$

$$\left(r \alpha_t \frac{\partial T}{\partial r} \right)_{r = r_{wb}} = 0, \tag{12}$$

and

$$T(r = r_e, t) = T_i, \tag{13}$$

To solve Eq. 1 numerically, we use the MacDonald and Coats (1970) procedure for generating a radial grid system. We divide the reservoir into geometrically spaced radial grid system generated by this procedure. Locating all the grid points at $r_{1/2} = r_w, r_{3/2}, \dots, r_{N_r+1/2}$, we have a total of N_r grid points. The outer boundary of the reservoir is represented by r_e which is the last gridblock boundary and taken very large to simulate an infinite-acting outer reservoir boundary.

2.2 Reservoir Pressure Equations

In deriving our semi-analytical and analytical solutions, we decouple temperature and pressure diffusivity equations when modeling sandface and wellbore temperatures by assuming that rock and fluid flow and thermal parameters do not change significantly with p and T. Such an approach has been shown to work as temperature changes are small for production and buildup tests: for example see, Duru and Horne (2010, 2011a,b); Palabiyik et al. 2016, Onur and Cinar (2017a). So, we can solve the pressure diffusivity equation for the skin and nonskin zone coupled with the appropriate initial and boundary conditions to obtain analytical expressions for computing time and spatial derivatives of pressure distribution in the left-hand side of Eq. 1. As stated before, we are interested in deriving solutions for constant rate or constant bottomhole pressure production cases. We will then use these constant-rate and constant-bottomhole pressure production responses in the superposition equations to be given later (see Eqs. 24 and 27) to generate the derivates of the pressures for the more general cases of specified variable rate and bottomhole pressure production.

For both constant-rate and constant-bottomhole pressure (BHP) production cases, we consider the same partial differential equations (PDEs), the initial reservoir condition (IRC) and outer reservoir boundary conditions (ORBC) given as follows:

The PDE that applies for the skin-zone is given by

$$\frac{1}{r}\frac{\partial}{\partial r}\left(r\frac{\partial p_S}{\partial r}\right)=\frac{1}{\eta_S}\frac{\partial p}{\partial t},\text{for } r_w<r<r_S \text{ and } t>0, \tag{14}$$

the PDE for the non-skin (or outer zone) is given by,

$$\frac{1}{r}\frac{\partial}{\partial r}\left(r\frac{\partial p_O}{\partial r}\right)=\frac{1}{\eta_O}\frac{\partial p_O}{\partial t},\text{for } r_S<r<\infty \text{ and } t>0, \tag{15}$$

the IRC is given by

$$p_S(r,t=0)=p_O(r,t=0)=p_i, \tag{16}$$

and the ORBC is given by

$$\lim_{r\to\infty} p_O(r,t>0)=p_i, \tag{17}$$

In addition to the conditions given by Eqs. 16 and 17, we need to have the following pressure and gradient continuity equations at the interface of the skin- and non-skin zones, given by, respectively,

$$p_S(r=r_S,t>0)=p_O(r=r_S,t>0), \tag{18}$$

and

$$\left(r\frac{\partial p_S}{\partial r}\right)_{r=r_S}=\left(r\frac{\partial p_O}{\partial r}\right)_{r=r_S}. \tag{19}$$

We consider production at either specified constant surface rate from the well

$$\left(r\frac{\partial p_S}{\partial r}\right)_{r=r_{wb}}=\frac{q_{sc}B_w}{2\pi\kappa_S h}, \tag{20}$$

or specified constant flowing bottomhole pressure given by the inner boundary condition as

$$p_S(r=r_{wb},t)=p_{wf}. \tag{21}$$

In Eqs. 14 and 15, η_S and η_O represent the diffusivity constant of the skin- and non-skin zones, given by, respectively,

$$\eta_S=\frac{k_S}{(\phi c_{Tw}\mu)_S}=\frac{\kappa_S}{(\phi c_{Tw})_S}, \tag{22}$$

and

$$\eta_O=\frac{k_w}{(\phi c_{Tw}\mu)_O}=\frac{\kappa_O}{(\phi c_{Tw})_O}, \tag{23}$$

where c_t is the effective isothermal compressibility of total system including rock and fluid. To solve the pressure diffusivity equations given by Eqs. 14-15 subject to initial and boundary conditions given by Eqs. 16-21, we use Laplace transformation. The solutions are lengthy and not given here. They can be found in Onur et al. (2017) and Onur and Ozdogan (2019). Although the solutions given by Onur et al. (2017) and Onur and Ozdogan (2019) are for slightly compressible oil systems, they can also be used for liquid-dominated geothermal systems. For the inverse Laplace transformation, we use Stehfest algorithm (1970). The Stehfest parameter used to evaluate the solutions is N_{stef} = 12 to obtain all our results given in this study.

To model temperature transient behavior under variable rate or variable BHP production cases, we use the well-known superposition principle. The pressure change at any point *r* and time *t* in the skin and outer zones can then be computed from the following superposition equation assuming piecewise step rate function in each time interval; i.e., q_j in the time interval from t_{j-1} to t_j for *j*=1,2,…,*N*, where *N* denotes the total number of flow rate steps:

$$p_i-p(r,t)=\sum_{j=1}^{N}(q_j-q_{j-1})\Delta p_u(r,t-t_{j-1}), \tag{24}$$

where $q_0=0$ and $t_0=0$,

$$p(r,t)=\begin{cases}p_S(r,t), & \text{if } r_w\le r\le r_S\\ p_O(r,t), & \text{if } r_S\le r<\infty\end{cases}, \tag{25}$$

and

$$\Delta p_u(r,t) = \begin{cases} \Delta p_{Su}(r,t), & \text{if } r_w \le r \le r_S \\ \Delta p_{Ou}(r,t), & \text{if } r_S \le r < \infty \end{cases} \quad (26)$$

In Eq. 24, $\Delta p_{Su}(r,t)$ and $\Delta p_{Ou}(r,t)$ represent the unit-rate pressure-change solutions at a point *r* inside the skin and non-skin zones, respectively. These unit-rate pressure-change solutions are computed from the solutions of the initial boundary value problem described by Eqs. 14-20. A. The derivatives of $p(r,t)$ with respect to *r* and *t* can be simply obtained by differentiation both sides of Eq. 16 with respect to *r* and *t* and then used in the right-hand side of Eq. 1 to model the sandface temperature transient under variable rate production from the well.

As to the specified variable BHP case, the pressure change at any point *r* and time *t* in the skin and outer zones can be computed from the following superposition equation assuming piecewise step bottomhole pressure-change function in each time interval; i.e., $\Delta p_{wf,j}$ in the time interval from t_{j-1} to t_j for *j*=1,2,…,*N*, where *N* denotes the total number of bottomhole pressure-change steps:

$$p_i - p(r,t) = \sum_{j=1}^{N} \left(\Delta p_{wf,j} - \Delta p_{wf,j-1}\right) \Delta p_{cp,u}\left(r, t - t_{j-1}\right), \quad (27)$$

where $q_0 = 0$ and $t_0 = 0$, and

$$\Delta p_{cp,u}(r,t) = \begin{cases} \Delta p_{cp,Su}(r,t), & \text{if } r_w \le r < r_S \\ \Delta p_{cp,Ou}(r,t), & \text{if } r_S < r \le \infty' \end{cases} \quad (28)$$

In Eq. 27, $\Delta p_{cp,Su}(r,t)$ and $\Delta p_{cp,Ou}(r,t)$ represent the unit-pressure-change solutions at a point *r* inside the skin and non-skin zones, respectively. These unit-pressure-change solutions are computed from the solutions computed from the solutions of the initial boundary value problem described by Eqs. 14-19 and 21. The derivatives of $p(r,t)$ with respect to *r* and *t* can be simply obtained by differentiation both sides of Eq. 27 with respect to *r* and *t* and then used in the right-hand side of Eq. 1 to model the sandface temperature transient under variable BHP production from the well.

Also, to solve the thermal energy balance equation (Eq. 1) subject to the initial and boundary conditions given by Eqs. 11-13 we use finite-difference method. The number of grid points which we use to discretize the reservoir in *r* -direction, is chosen as 200 after the sensitivity analysis of gridblock number not given here. The details of the numerical solution of Eq. 1 subject to the conditions given by Eqs. 11-13 can be found in Onur et al. (2017) and Onur and Ozdogan (2019).

3. ANALYTICAL SANDFACE TEMPERATURE SOLUTIONS

The semi-analytic formulation given in the previous section is quite general for predicting sandface temperature transient behavior for more general cases; variable rate, variable BHP, including conduction and convection for each flow period including buildup periods. Although the semi-analytical and numerical solutions are more general and rigorous, they are not in closed and explicit form revealing analytically the effects of various parameters affecting the sandface temperature, and also performing nonlinear parameter estimation based on semi-analytical and numerical solutions. Also, the accuracy of these solutions are strongly dependent on the spatial grid and time steps used. Here, we provide analytical solutions for constant rate drawdown and buildup periods. These analytical solutions, although approximate, provide better understanding and identification of the parameters effecting constant rate drawdown and buildup sandface temperatures.

3.2 Constant-Rate Drawdown Solution

Recently, Panini et al. (2019) presented an approximate analytical solution for predicting drawdown temperature transient behavior of a fully penetrating vertical well in a two-zone radial composite reservoir system shown in Fig. 3. Although their solution is for a single-phase flow of oil with presence of immobile water, their solution can easily be adapted to single-phase flow of water composite system. Their solution adapted for the liquid-dominated single-phase water system here is given by

$$T_{sf}(t) = T_i + a_S\left(\varphi^*_{St} - \varepsilon_{JTS}\right)\int_{\frac{r_S^2}{4\eta_S t}}^{\frac{r_w^2}{4\eta_S t}} \frac{e^{-z}}{z + b_S e^{-z}}dz - a_S\varphi^*_{St}\left(1 - \frac{\kappa_S}{\kappa_O}\right)\int_{\frac{r_S^2}{4\eta_S t}}^{\frac{r_w^2}{4\eta_S t}} \frac{e^{-z\frac{r_S^2}{r_w^2}}}{z + b_S e^{-z}}dz$$
$$- a_S\varphi^*_{St}\frac{\kappa_S}{\kappa_O}\frac{r_S^2}{r_{wb}^2}\left(1 - \frac{\eta_S}{\eta_O}\right)\int_{\frac{r_S^2}{4\eta_S t}}^{\frac{r_{wb}^2}{4\eta_S t}} \frac{e^{-z\frac{r_S^2}{r_{wb}^2}\left(1-\frac{\eta_S}{\eta_O}\right)}}{z + b_S e^{-z}} z\,\mathrm{Ei}\left(-z\frac{\eta_S}{\eta_O}\frac{r_S^2}{r_{wb}^2}\right)dz$$
$$+ \varepsilon_{JTS}a_S\left[\mathrm{Ei}\left(-\frac{r_{wb}^2}{4\eta_S t}\right) - \mathrm{Ei}\left(-\frac{r_S^2}{4\eta_S t}\right)\right]$$
$$+ a_O\varphi^*_{Ot}\frac{r_S^2}{r_{wb}^2}\left(1 - \frac{\eta_S}{\eta_O}\right)\int_{\frac{r_S^2}{4\eta_S t}}^{\infty} \frac{z e^{-z\frac{r_S^2}{r_{wb}^2}\left(1-\frac{\eta_S}{\eta_O}\right)}}{z + b_O e^{-z\left(\frac{r_S^2}{r_{wb}^2} - \frac{r_S^2}{r_{wb}^2}\frac{\eta_S}{\eta_O} + \frac{\eta_S}{\eta_O}\right)}} \mathrm{Ei}\left(-z\frac{\eta_S}{\eta_O}\right)dz'$$
$$+ a_O\left(\varphi^*_{Ot} + \varepsilon_{JTw}\right)\int_{\frac{r_S^2}{4\eta_S t}}^{\infty} \frac{e^{-z\left(\frac{r_S^2}{r_{bw}^2} - \frac{r_S^2}{r_{wb}^2}\frac{\eta_S}{\eta_O} + \frac{\eta_S}{\eta_O}\right)}}{z + b_O e^{-z\left(\frac{r_S^2}{r_{bw}^2} - \frac{r_S^2}{r_{wb}^2}\frac{\eta_S}{\eta_O} + \frac{\eta_S}{\eta_O}\right)}} dz$$
$$+ \varepsilon_{JTw}a_O\,\mathrm{Ei}\left[-\frac{r_S^2}{4\eta_S t}\left(\frac{r_S^2}{r_{wb}^2} - \frac{r_S^2}{r_{wb}^2}\frac{\eta_S}{\eta_O} + \frac{\eta_S}{\eta_O}\right)\right], \tag{29}$$

where

$$a_S = \frac{q_{scw}B_w}{4\pi\kappa_S h}, \tag{30}$$

$$b_S = a_S c_{SpR}\frac{\kappa_S}{\eta_S}, \tag{31}$$

$$a_O = \frac{q_{scw}B_o}{4\pi\kappa_O h}, \tag{32}$$

and

$$b_O = a_O c_{OpR}\frac{\kappa_O}{\eta_S}. \tag{33}$$

In Eq. 29, $\mathrm{Ei}(-x)$ represents the exponential integral function (Abramowitz and Stegun, 1972). We compute the integrals in Eq. 39 by numerical integration using Gauss-Kronrod quadrature method with 21 points.

The nice thing about the solution given by Eq. 29 is that it incorporates effect of skin zone on the temperature behavior. The individual skin zone properties such as k_S and r_S have profound effects on the drawdown sandface temperatures as discussed by Duru and Horne (2011b), Palabiyik et al. (2016), and Onur and Cinar (2017b). Onur and Cinar (2017a) presented also approximate analytical equations for predicting sandface temperatures for a single-layer system incorporating the skin effect as a lumped parameter. Their analytical solution that is applicable for late times such that

$$t > \frac{20\pi r_{wb}^2 h}{c_{OpR}q_{scw}B_w}, \tag{34}$$

when temperature diffusion propagates out the skin zone is given by

$$T_{sf}(t) = T_i + m_{TlD}\left[\log(t) + \log\left(\frac{4\eta_O}{e^\gamma r_{wb}^2}\right) + 0.869S - \left(\frac{\varphi^*_{Ot} - \varepsilon_{JTw}}{\varepsilon_{JTw}}\right)\log\left(\frac{e^\gamma c_{OpR}\,q_{scw}B_w}{4\pi\eta_O h}\right)\right], \tag{35}$$

where $\gamma\ (= 0.577215\ldots)$ is Euler's constant and m_{TlD} is given by

$$m_{TlD} = -0.183\frac{q_{scw}B_w\varepsilon_{JTw}}{\kappa_O h}. \tag{36}$$

Eq. 29 at late times reduce to Eq. 35, and at early times such that

$$\frac{25r_{wb}^2}{\eta_S} < t < \frac{\pi r_{wb}^2 h}{20c_{SpR}q_{scw}B_w}, \tag{37}$$

it reduces to

$$T_{sf}(t) = T_i - m_{TeD}\left[\log(t) + \log\left(\frac{4\eta_S}{e^\gamma r_w^2}\right)\right], \tag{38}$$

where γ $(= 0.577215 \ldots)$ is Euler's constant and m_{TlD} is given by

$$m_{TeD} = 0.183 \frac{q_{scw} B_w \varphi^*_{Ot}}{\kappa_S h}. \tag{39}$$

3.3 Buildup Solution

Onur et al. (2019) has very recently presented an approximate analytical solution for predicting buildup temperature transient behavior of a fully penetrating vertical well in a two-zone radial composite reservoir system shown in Fig. 3. This solution is quite complex and hence we do not present here. It can be found in Onur et al. (2019). As the solution for no skin zone case is simpler, we record this solution here. This solution was first presented for Galvao (2018) (also see Galvao et al., 2019) for a single-phase oil with presence of immobile water system. Onur et al. (2019) solution for zero skin case reduces to Galvao et al. (2019) solution, which can be expressed for a liquid-dominated geothermal system as

$$T_{sf}(\Delta t) = T_{sf}(\Delta t = 0) + \frac{q_{scw} B_w}{2\kappa_O h} \left\{ \frac{\varphi^*_{Ot}}{\left(1 - \frac{\alpha_t}{\eta_O}\right)} \left[-\mathrm{Ei}\left(-\frac{r_w^2}{4\eta_O \Delta t} \right) + \mathrm{Ei}\left(-\frac{r_w^2}{4\alpha_t \Delta t} \right) \right] - \varepsilon_{JTw} \mathrm{Ei}\left(-\frac{r_w^2}{4\alpha_t \Delta t} \right) \right\}, \tag{40}$$

where $T_{sf}(\Delta t = 0)$ is the sandface temperature at the moment of shut-in.

4. WELLBORE TEMPERATURE SOLUTIONS

There are a multitude of papers proposed in the literature for predicting wellbore temperature at a point above the feed or producing zone (see Fig. 3). Both numerical as well as analytical models have been proposed. Most of the analytical models proposed assume isothermal flow in the reservoir and steady-state heat flow in the wellbore; e.g., Ramey (1962), Curtis and Witterholt (1973), Alves et al. (1992), Hasan and Kabir (1994).

Hasan et al. (2005) were the first to present an analytical wellbore-temperature equation for predicting transient wellbore temperature along the wellbore for drawdown and buildup tests under single-phase fluid flow in the wellbore. They considered the effects of steady-state momentum and J-T effects. Later, Izgec et al. (2007) presented an improved version of the Hasan et al. (2015) analytical and pointed out that the constant overall-heat-transfer-coefficient assumption in the analytical fluid temperature model of Hasan et al. (2005) may not be reasonable for early transients, especially in drawdown. There are also models based on discretization of wellbore for predicting transient wellbore temperature distribution for single phase flow of fluid along the wellbore by considering transient mass, momentum, and energy balance equations, but considering isothermal flow in the reservoir. For instance, the models of Miller (1980), and Hasan et al. (1997) are examples of such numerical models.

In all works cited above, the reservoir models used assume isothermal flow so that the bottomhole temperature within the vertical wellbore across from the producing horizon temperature is equal to the initial reservoir geothermal temperature, which is constant, i.e., not changing with time. Only a few works have treated the reservoir flow as nonisothermal so that the sandface or bottomhole temperature changes with time due to conduction, convection, adiabatic expansion and J-T effects in the reservoir are coupled with a nonisothermal flow in the wellbore. For instance, Duru and Horne (2010a) used their nonisothermal reservoir flow model to predict bottomhole temperature as a function of time and then input this temperature into the their modified version of the transient wellbore-temperature model of Hasan et al. (2005) without momentum and J-T effects in the wellbore. A similar approach to that of Duru and Horne (2010a) is followed by Onur et al. (2017b) who arrived at a more accurate equation for wellbore temperature. Duru and Horne (2010a) did not present the derivation of their modified version of the equation. Sui et al. (2008a) and Sidorova et al. (2015) also considered a nonisothermal reservoir flow model coupled with a discretized nonisothermal wellbore model assuming steady-state mass, momentum and thermal energy balance equations. Onur et al. (2017) also included the effects of transient flow rate and pressure distribution along the wellbore obtained by solving a combined unsteady state mass and momentum balance equation analytically. Onur et al. (2017) solution can also be used with uniform flow rate distribution along the wellbore for constant-rate drawdown tests or zero flow rate distribution for buildup tests with negligible wellbore storage and momentum effects.

Recently, Galvao (2018) and Galvao et al. (2019) presented an improved version of the Onur et al. (2017) analytical solution for predicting wellbore temperature distribution. Their model accounts for Joule-Thomson, adiabatic fluid-expansion, conduction and convection effects. The wellbore fluid mass density is modeled as a function of temperature, and the analytical solution makes use of the Laplace transformation to solve the transient heat-flow differential equation, accounting for a transient wellbore-temperature gradient $\partial T/\partial z$. However, their solution assumes that the volumetric rate along the wellbore is uniform flow rate distribution along the wellbore, and therefore wellbore storage and momentum effects along the wellbore are neglected in the Galvao et al. (2019) solution, but wellbore pressure distribution were treated as variable with density of water changing solely with temperature (see Eq. 55).

There are also coupled transient wellbore/reservoir-temperature numerical models where both the reservoir and wellbore mass, momentum, and energy balance equations are solved simultaneously. For example, Kutun et al. (2014) presented a numerical model to study the parameters effecting the stabilization time of static and dynamic conditions in the wells for a single-phase water system. The model is based on mass and energy balance equations and couples the reservoir with the well and considers the heat losses to the surroundings of the well. However, the well is treated as a reservoir block in their model and does not consider momentum effects.

In this study, we compare the results generated from the analytical solutions of Onur et al. (2017) without momentum effects and Galvao et al. (2019). We first present the Onur et al. (2017) and then the Galvao et al. (2019) analytical solutions which can be used to predict wellbore temperature for both production and shut-in periods.

4.1 Onur et al. (2017b) Analytical Wellbore Temperature Solutions

Onur et al. (2017) presented a solution based on the following based on the following energy balance equation to predict the transient wellbore-temperature distribution in the wellbore [denoted by $T_w(z,\Delta t_j)$]:

$$\frac{1}{a_j}\frac{\partial T_{wj}}{\partial \Delta t_j} = L_R\left[T_{ei}(z) - T_{wj}\left(z,\Delta t_j\right)\right] - \left[\frac{\partial T_{wj}}{\partial z} - \Phi\left(p_{wj},T_{wj}\right) + \frac{g\sin\theta}{g_c c_{p_{wb}} J}\right], \tag{41}$$

where Δt_j is the elapse time given from a begining of a flow period j, i.e., $t_j = t - t_{pj}$, where t is the total time since the beginning of the first flow period, and t_{pj} is the time at the beginning of the flow period j; either constant-rate production or buildup following a constant-rate production. In Eq. 41. a_j is given by

$$a_j = \frac{q_{wj}}{A_w(1+C_T)}, \tag{42}$$

where q_{wj} is the volumetric flow rate at bottomhole conditions for the flow period j, A_w is the cross-sectional area of the wellbore perpendicular to fluid flow, and g_c and J are the unit conversion factors. As we use the SI unit system, g_c and J are equal to unity. C_T is a lumped parameter and referred to as the thermal storage parameter (dimensionless) introduced by Hasan et al. (2005) and defined as the ratio of internal energy per unit length of the wellbore to the internal energy of the fluid per length. In our applications given in this paper, we set $C_T = 0$. In Eq. 41, the parameter $\Phi(p_w,T_w)$ is given by

$$\Phi\left(p_{wj},T_{wj}\right) = \varepsilon_{JTwb}\frac{\partial p_{wj}}{\partial z} - \frac{q_{wj}}{A_w^2 g_c c_{p_{wb}} J}\frac{\partial q_{wj}}{\partial z}. \tag{43}$$

In Eq. 41, $T_{ei}(z)$ is the initial earth temperature distribution due to geothermal gradient, defined by

$$T_{ei}(z) = T_{eibh} - z g_G \sin\theta_w, \tag{44}$$

where T_{eibh} is the earth temperature at $z = 0$ and $t = 0$, g_G is the geothermal gradient in K/m. The solution of Eq. 41 for a multi-rate history is given by (Onur et al. 2017; Onur and Cinar 2017b):

$$\begin{aligned} T_{wj}\left(z,\Delta t_j\right) = {} & e^{-aL_R\Delta t_j}T_{wf}\left(z,t_{pj}\right) + \left(1-e^{-aL_R\Delta t_j}\right)\left\{T_{ei}(z) + e^{-aL_Rz}\left[T_{bh}\left(\Delta t_j\right) - T_{eibh}\right]\right\} \\ & - e^{-aL_Rz}\frac{\left(1-e^{-aL_R\Delta t_j}\right)}{L_R}\psi\left(z,\Delta t_j\right), \end{aligned} \tag{45}$$

where $T_{bh}(\Delta t_j)$ is the bottomhole temperature to be computed from the semin-analytical solutions of Eq. 1 or its approximate sandface solutions for constant rate and buildup as a function of time, and

$$\psi\left(z,\Delta t_j\right) = g\sin\theta_w + \varepsilon_{JTwb}\frac{\partial p_{wj}}{\partial z} - \frac{q_{wj}}{A_w^2 g_c c_{p_{wb}} J}\frac{\partial q_{wj}}{\partial z} - \frac{g\sin\theta_w}{g_c c_{p_{wb}} J}, \tag{46}$$

where ε_{JTwb} and $c_{p_{wb}}$ are J-T coefficient and specific heat capacity of the wellbore fluid. θ_w is the inclination angle of the wellbore measured from the horizontal; $\theta_w = 90^o$ is for a vertical wellbore.

In Eq. 45, $T_{wf}\left(z,t_{pj}\right)$ is the wellbore-temperature distribution at the time t_{pj}, i.e., at the onset of flow period j. For the first flow period, T_{wf} is taken as T_{ei}. In Eqs. 41 and 44, L_R is referred to as the "relaxation distance," defined by:

$$L_R\left(\Delta t_j\right) = \frac{2\pi r_{co}U_t\lambda_e}{\rho_{wb}q_{wj}c_{p_{wb}}\left[\lambda_e + r_{co}U_t f_D\left(\Delta t_j\right)\right]}, \tag{47}$$

where $f_D(\Delta t_{Dj})$ is the dimensionless heat transfer function which is given by (Hasan and Kabir 2002):

$$f_D\left(\Delta t_j\right) = \ln\left[e^{-0.2\Delta t_j} + \left(1.5 - 0.3719e^{-\Delta t_j}\right)\sqrt{\Delta t_j}\right], \tag{48}$$

where t_D represents the dimensionless time defined by

$$\Delta t_{Dj} = \frac{\alpha_{te}}{r_{co}^2}, \tag{49}$$

where α_{te} is the effective/total thermal diffusivity constant of earth. In Eq. 46, U_t is the overall heat transfer coefficient, which determines the heat transfer from the wellbore to the sorroundings, computed from (Sagar et al. 1991):

$$U_t = \frac{1}{r_{co}}\frac{\lambda_{cem}}{\ln(r_{wb}/r_{co})}, \tag{50}$$

for a case where flow occurs inside a production casing. It is important to note that the above equations can be used with momentum and wellbore storage effects, as shown by Onur et al. (2017). In this case, flow rate and pressure distribution along the wellbore is computed from isothermal momentum equation for single-phase flow, see Onur et al. for details.

It is worth noting that we assume that fluid inside the wellbore and fluid in the reservoir have identical physical properties: i.e., $\varepsilon_{JTwb} = \varepsilon_{JTw}$, $c_{p_{wb}} = c_{p_w}$, $\rho_{wb} = \rho_w$, etc.

4.2 Galvao et al. (2019) Analytical Wellbore Temperature Solutions

Galvao et al. (2019) used the same energy balance equation (Eq. 41) considered by Onur et al. (2017), but expressed in terms of temperature change defined by

$$\Delta T_{wj}(z,\Delta t_j) = T_{wj}(z,\Delta t_j) - T_{ei}(z) = T_{wj}(z,\Delta t_j) - T_{eibh} + z g_G \sin\theta_w, \tag{51}$$

So that Eq. 41 can be written as

$$\frac{1}{a}\frac{\partial \Delta T_{wj}}{\partial \Delta t_j} = L_R \Delta T_{wj} - \left[\frac{\partial \Delta T_{wj}}{\partial z} - g_G \sin\theta_w - \Phi(p_{wj},T_{wj}) + \frac{g\sin\theta_w}{g_c c_{p_{wb}} J}\right]. \tag{52}$$

However, they considered only constant rate drawdown and buildup period following a constant-rate drawdown period. Note they neglected wellbore storage and skin effects so that we can assume a uniform volumetric flow rate so that the parameter $\Phi(p_w,T_w)$ reduces to

$$\Phi(p_{wj},T_{wj}) = \varepsilon_{JTwb}\frac{\partial p_{wj}}{\partial z} = -\varepsilon_{JTwb}\frac{g\,\rho_{wb}(p_{wj},T_{wj})\sin\theta_w}{g_c} = -\varepsilon_{JTwb}\gamma_{wb}(p_{wj},T_{wj}). \tag{53}$$

They use Eq. 53 in Eq. 52 to obtain:

$$\frac{1}{a}\frac{\partial \Delta T_{wj}}{\partial \Delta t_j} = L_R \Delta T_{wj} - \left[\frac{\partial \Delta T_{wj}}{\partial z} - g_G \sin\theta_w + \varepsilon_{JTwb}\gamma_{wb}(p_{wj},T_{wj}) + \frac{g\sin\theta_w}{g_c c_{p_{wb}} J}\right]. \tag{54}$$

They treat density or the specific weight of the wellbore fluid (in our case it is water or brine) as a function of only temperature so that the specific weight of the wellbore fluid can be expressed in term of the isobaric-thermal-expansion coefficient (β_w) as

$$\gamma_{wb}(p_{wj},T_{wj}) = \gamma_{wbi}\left[1 - \beta_w\left(\Delta T_{wj} - z g_G \sin\theta_w\right)\right], \tag{55}$$

where γ_{wbi} is the reference specific weight of wellbore fluid (water), evaluated at initial temperature T_{eibh} and initial pressure p_i at $z = 0$. Using Eq. 55 in Eq. 54 and defining a new "relaxation-distance-parameter" L_β as

$$L_\beta = L_R - \gamma_{wbi}\beta_w\varepsilon_{JTwb}, \tag{56}$$

we can express Eq. 54 as

$$\frac{1}{a}\frac{\partial \Delta T_{wj}}{\partial \Delta t_j} = -L_\beta \Delta T_{wj} - \frac{\partial \Delta T_{wj}}{\partial z} - z\Omega + \psi, \tag{57}$$

where

$$\Omega = \gamma_{wbi}\beta_w\varepsilon_{JTwb}\sin\theta_w, \tag{58}$$

and

$$\psi = g\sin\theta_w + \gamma_{wbi}\varepsilon_{JTwb} - \frac{g\sin\theta_w}{g_c c_{p_{wb}} J}. \tag{59}$$

The solution of Eq. 57 subject to the initial and boundary condition, given respectively, by

$$\Delta T_{wj}(z,\Delta t_j = 0) = 0, \tag{60}$$

and

$$\Delta T_{wj}(z = 0,\Delta t_j) = T_{sf}(\Delta t_j). \tag{61}$$

for a constant-rate drawdown period is obtained as

$$\Delta T_{wj}(z,\Delta t_j) = T_{sf}\left(\Delta t_j - \frac{z}{a}\right)e^{-zL_\beta}H\left(\Delta t_j - \frac{z}{a}\right) + \frac{1}{L_\beta^2}\Big\{H\left(\Delta t_j - \frac{z}{a}\right)\left[e^{-aL_\beta\Delta t_j}\left(a\Omega L_\beta\Delta t_j - z\Omega L_\beta + \Omega + \psi L_\beta\right)\right] - e^{-aL_\beta\Delta t_j}\left(a\Omega L_\beta\Delta t_j - z\Omega L_\beta + \Omega + \psi L_\beta\right) - H\left(\Delta t_j - \frac{z}{a}\right)e^{-zL_\beta}\left(\Omega + \psi L_\beta\right) + \Omega(1 - zL_\beta) + \psi L_\beta\Big\} \quad (62)$$

Their wellbore temperature solution for the buildup period (following a constant-rate drawdown) is given by

$$\Delta T_{wsj}(z,\Delta t_j) = e^{-aL_R\Delta t_j}\left[T_{wf}(z,t_{pj}) + \Delta T_{sf}(\Delta t_j = 0^+)\right] \quad (63)$$

where $T_{wf}(z,t_{pj})$ is the wellbore temperature at moment of shut-in at the gauge depth of z, which is computed from Eq. 62 with $\Delta t_j = t_{pj}$ and $\Delta T_{sf}(\Delta t_j = 0^+)$ is sandface temperature change computed from Eq. 40 for a small dt equal a value from 1 to 5 seconds to account for immediate impact of shutting in the well (i.e., the heating response caused by the adiabatic fluid compression.

5. COMPARISION OF SANDFACE AND WELLBORE TEMPERATURE SOLUTIONS

Here, we compare our sandface and wellbore temperatures computed from analytical, semi-analytical, and numerical solutions.

5.1 Sandface Temperature Solutions

We consider the same synthetic drawdown and buildup case considered in Palabiyik et al. (2016). The input data used in computations are given in Table 1. We consider two different values of the skin factor; $S = 0$ and 5. However, for the case of $S = 5$, as shown in Table 2, we vary r_S and k_S to show the individual effects of these two skin zone parameters on transient temperature responses. The simulated test sequences consist of a 5-day production at a constant mass rate of 40 kg/s (or = sm^3/s) followed by a 15-day buildup. The outer reservoir radius r_e is chosen large enough so that the system acts as infinite acting during the total duration of the test.

Shown in Figs. 4 are comparisons of sandface drawdown solutions computed from the analytical equation given by Eq. 29 (Panini et al. 2019), the semi-analytical solution of Eq. 1 (Onur et al. 2017), and CMG-STARS for Case 1 ($S = 0$) and Case 2 ($S = 5, r_S = 1.06$ m), while shown in Figs. 5 are comparisons of buildup solutions from the same solutions for the same two skin cases. As can be seen, all three solutions are in close agreement, though sandface temperatures computed from the semi-analytical solution of Onur et al. (2017) agree better with the more rigorous CMG-STARS solution.

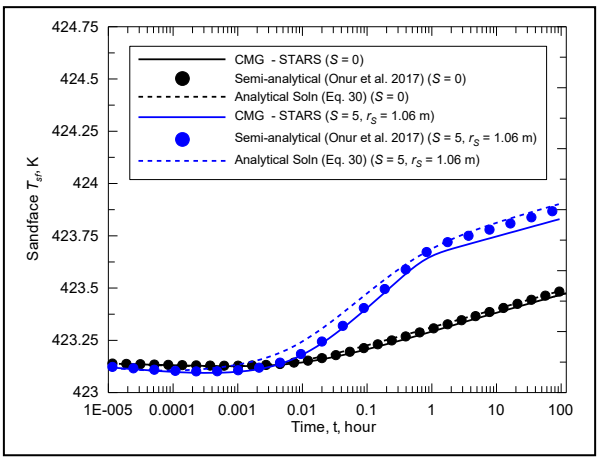

Figure 4: Comparison of sandface temperature solutions for drawdown.

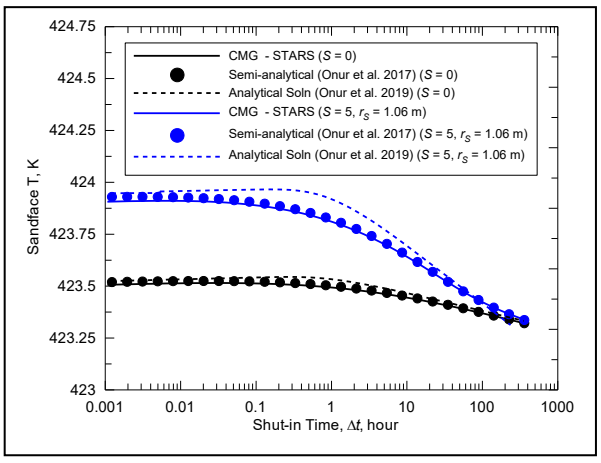

Figure 5: Comparison of sandface temperature solutions for buildup.

Table 1 — Input parameters for synthetic drawdown and buildup test; (a) fluid properties, (b) rock properties, and (c) wellbore and reservoir parameters.

(a) Fluid properties input data.

Parameter	Value
T_i (K)	423.15
p_i (MPa)	12.5
ρ_w (kg/m^3)	923.68
B_w (m^3/sm^3)	1.08
c_{Tw} (Pa^{-1})	5.868×10^{-10}
β_{pw} (K^{-1})	9.853×10^{-4}
μ_w (Pa.s)	1.855×10^{-4}
ε_{JTw} (K/Pa)	-1.478×10^{-7}
φ_w (K/Pa)	1.057×10^{-7}
c_{pw} (J/kg-K)	4269.9

(b) Rock properties input data.

Parameter	Value
k (m^2)	4.935×10^{-14}
k_S (m^2)	variable
ϕ (fraction)	0.10
h (m)	50
ρ_s (kg/m^3)	2650
c_{ps} (J/kg-K)	1000
c_{Tr} (Pa^{-1})	0.0
β_{pr} (K^{-1})	0.0
λ_{tr} (J/m-s-K)	2.92
c_{ptr} (J/m^3-K)	2.779×10^{6}
$\phi c_{Tr} h$ (m/Pa)	2.934×10^{-9}

(c) Wellbore data and reservoir.

Parameter	Value
r_{wb} (m)	0.1
r_S (m)	variable
r_e (m)	25,000
S (dimensionless)	variable
q_{scw} (sm^3/s)	4×10^{-2}
$(\rho c_p)_{tr}$ (J/m^3-K)	2.779×10^{6}
c_{pR} (dimensionless)	1.419
φ_t^* (K/Pa)	1.500×10^{-8}
α_{tr} (m^2/s)	1.051×10^{-6}
λ_e [J/m-s-K]	1.731
λ_{cem} [J/m-s-K]	0.346
α_e [m/s]	7.3806×10^{-7}
g_G [K/m]	0.10
g [m/s^2]	9.80665
L_w [m]	1300
θ^w [°]	90
r_{ci} [m]	0.0692
r_{co} [m]	0.0782
D [m]	0.1385
T_{eiwh} [K]	293.15
T_{eibh} [K]	423.15
C_T [dimensionless]	0

Table 2 ─ Skin zone parameters.

Skin Cases	Skin factor, S (unitless)	k (m^2)	k_S (m^2)	r_S (m)
Case 1	0	4.935×10^{-14}	4.935×10^{-14}	0.1
Case 2	5	4.935×10^{-14}	1.583×10^{-14}	1.06
Case 3	5	4.935×10^{-14}	8.186×10^{-15}	0.27

5.2 Wellbore Temperature Solutions

Here, we compare the wellbore temperatures computed from the Onur et al. (2017) and Galvao et al. (2019) solutions at three different gauge locations for both drawdown and buildup periods for the case of zero skin (Case 1 of Table 2). Fig. 6 shows a comparison for the drawdown period for three different gauge locations; $z_g = 0$, 50 and 500 m, while Fig. 7 shows a comparison for the buildup period for the same gauge locations. For the results shown in Figs. 6 and 7, we used the sandface solutions computed from the Onur et al. semi-analytical solution. As can be seen, there is a big difference between the two solutions at early times. As mentioned before, the main differences between these two solutions are due to their treatment of a transient wellbore-temperature gradient $\partial T/\partial z$ when solving Eq. 41 (or equivalently Eq. 51) and the treatment of density of the fluid. Onur et al. 2017 assumes density is constant, while Galvao et al. (2019) treats density as of function temperature (see Eq. 55). Hence, we expect the Galvao et al. solution (Eq. 45) is more accurate over the Onur et al. solution (Eq. 52) if both solutions are evaluated by assuming constant rate for the drawdown period and zero rate for buildup period. Although not shown here, we have compared the Onur et al. (2017) and Galvao et al. (2019) solutions for Cases 2 and 3 and obtained similar conclusions to that of zero skin case shown in Figs. 6 and 7.

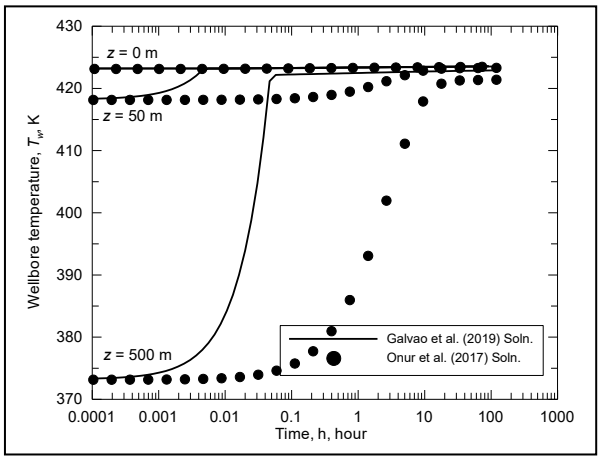

Figure 6: Comparison of wellbore temperature solutions for drawdown at three different gauge locations

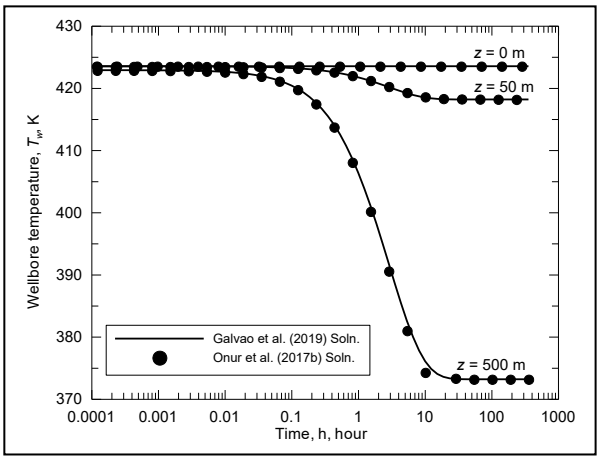

Figure 7: Comparison of wellbore temperature solutions for buildup at three different gauge locations.

6. FLOW REGIMES EXHIBITED BY SANDFACE & WELLBORE TEMPERATURE DATA

Here, we present and investigate sandface and wellbore temperature transient behaviors of a vertical well producing in infinite-acting two-zone radial composite reservoirs at a specified constant. Unless otherwise stated, we consider our reference case (Tables 1 and 2) to generate our results for a constant-rate drawdown period and buildup period following a constant-rate drawdown period, considered in the previous section. Here, we only present results for constant-rate drawdown and buildup cases. The constant bottom-hole pressure (BHP), variable rate and variable rate production cases can be found in Bircan (2020) and Alan (2020).

6.1 Sandface Temperature Solutions

As discussed in Section 3, Onur et al. (2016) identified the flow regimes which may be exhibited by the sandface temperature transient data for a fully-penetrating well producing at a specified constant rate with and without skin effects. Their study only considered an infinite-acting homogeneous reservoir system. Based on Onur et al. (2016), sandface temperature data for this case may exhibit three radial-flow regimes; (i) early-time radial flow occurring at very early times of flowing time, (ii) intermediate radial flow occurring at the intermediate times if there is a skin zone adjacent to the wellbore, and (iii) late-time radial flow occurring at late flowing times. Onur et al. (2016) presented the approximate equations for each of these three flow regimes mentioned above, which aid analysis of temperature transient data to infer various fluid and heat flow related reservoir parameters of interest, such as porosity, permeability, skin zone radius, Joule-Thomson coefficient, from temperature transient data. These equations are given previously in Section 3.

For flow regime identification purposes from temperature data, Onur et al. (2016) and Onur and Cinar (2017a) propose to use the following derivative function for flow regime identification:

$$abs\left(\frac{d\Delta T_{wf}}{d\ln t}\right) = \left| t\,\frac{d\Delta T_{wf}}{dt} \right|, \tag{64}$$

where T_{wf} can represent either the sandface temperature ($z_g = 0$) or the wellbore temperature ($z_g > 0$). We simply refer it to as the temperature-derivative. Fig. 8 shows log-log diagnostic plots of absolute value of temperature-derivative data versus flowing time for the infinite-acting with and without skin cases of Table 2. Fig. 8 presents only the results for drawdown response. For the same cases, the derivatives of sandface temperature for buildup period for the same test case can be found in Onur et al. (2016). As seen from Fig. 8, temperature-derivative data without skin zone for an infinite-acting reservoir case identifies three flow regimes: (i) early-time IARF reflecting non-skin zone properties, and (ii) late-time IARF. In Fig. 9, a semilog plot of sandface drawdown temperatures with and without skin cases of Table 2 is shown. As also shown in Figs. 8 and 9, when there exists a skin zone, temperature-derivative data show early-time IARF and intermediate-IARF with zero-slope lines reflecting the skin zone properties as discussed before. The late-time flow regime observed reflects non-skin zone properties, as given by Eq. 35. It is worth noting that if temperature data exhibit all three flow regimes, we can estimate skin zone properties such as k_S and r_S, J-T coefficient, thermal diffusivity/conductivity of the total system, and the non-skin zone permeability. However, we should note that thermal diffusivity/conductivity of the total system cannot be estimated reliably from the sandface temperature data as such data are not sensitive to the thermal diffusivity/conductivity. Sandface buildup data show more sensitivity to the thermal diffusivity, see Eq. 40. Another important remark is that the skin zone parameters k_S and r_S cannot be estimated from transient pressure data alone as diffusion of pressure transient data is much faster than that of temperature transient data. For example, as can be seen from Figs. 8 and 9, the skin zone affects the sandface temperature responses until about 0.2 hours for $r_S = 0.27$ m case and 5 hours for $r_S = 1.06$ m case. Although not shown here, the effect of skin zone on pressure transient responses are not observable after 0.01 hours.

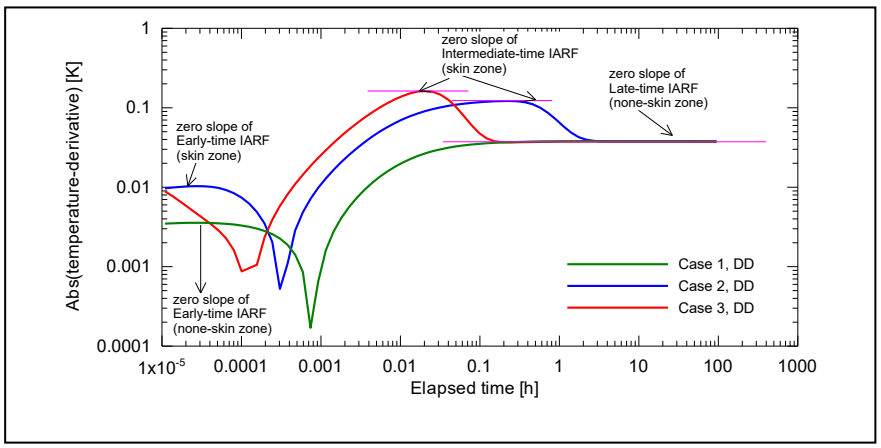

Figure 8: Log-log diagnostic plots of temperature-derivative versus time for constant-rate drawdown test with three different skin cases of Table 2.

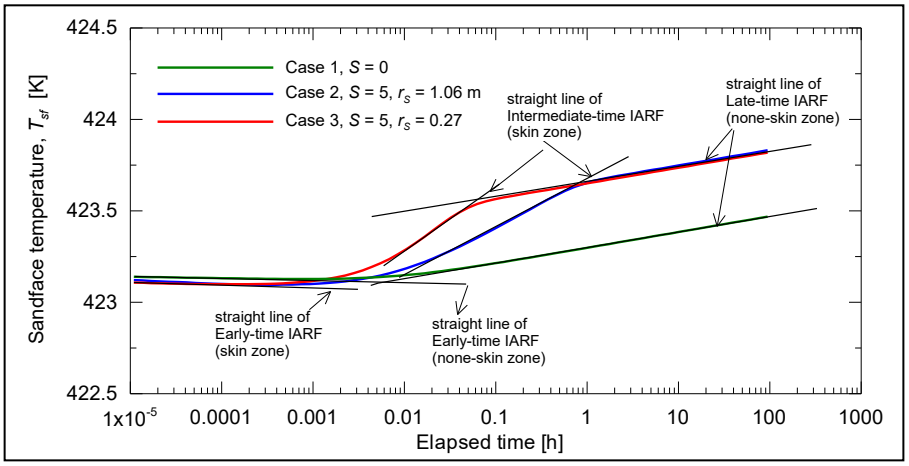

Figure 9: Semi-log plots of temperature-derivative versus time for constant-rate drawdown test with the three different skin cases of Table 2.

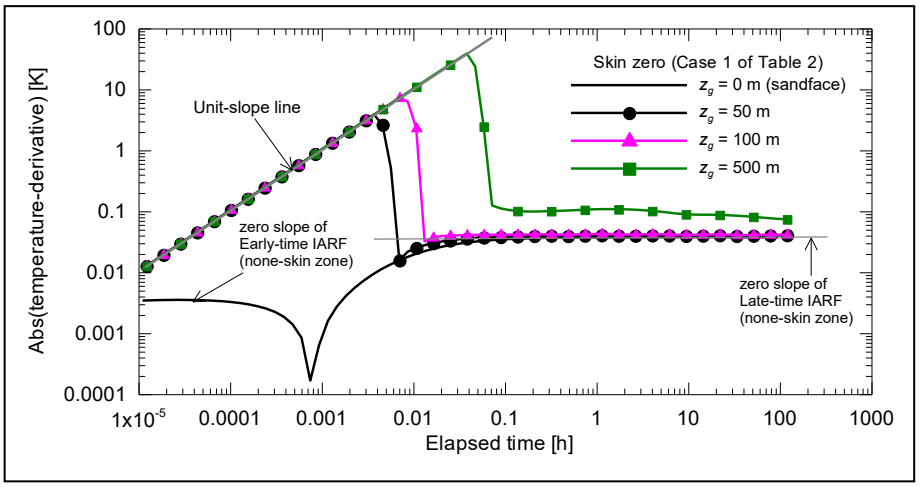

Figure 10: Log-log diagnostic plots of wellbore temperature-derivative versus time for constant-rate drawdown test for four different gauge locations in the wellbore, Case 1 (zero skin) of Table 2.

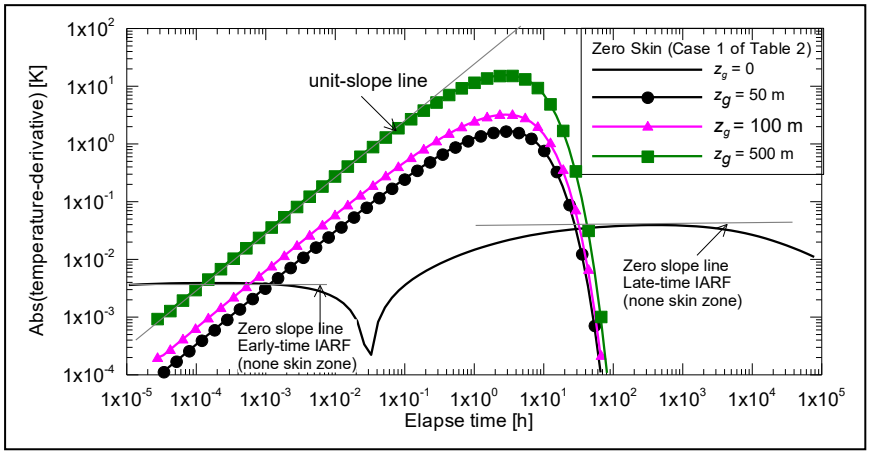

Figure 11: Log-log diagnostic plots of wellbore temperature-derivative versus time for buildup test for four different gauge locations in the wellbore, Case 1 (zero skin) of Table 2.

.

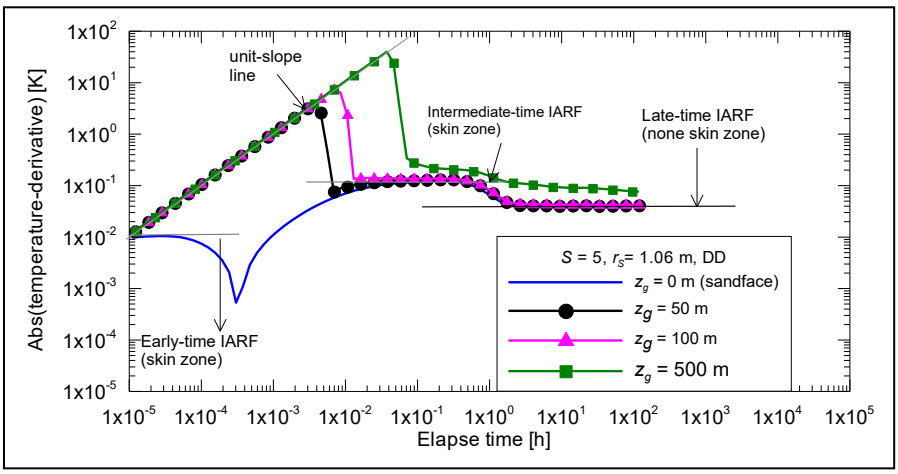

Figure 12: Log-log diagnostic plots of wellbore temperature-derivative versus time for drawdown test for four different gauge locations in the wellbore, Case 2 (non-zero skin) of Table 2.

6.2 Wellbore Temperature Solutions

To investigate the flow regimes exhibited by the wellbore temperatures data measured at gauge locations above the sandface or feed zone, we inspect the log-log diagnostic plots of wellbore temperature derivatives as shown in Fig. 10 for drawdown and in Fig. 11 for buildup periods. We have used the Galvao et al. (2019) analytical solutions given by Eq. 62 and 63. As can be seen, drawdown derivative response contains more information as to the reservoir parameters than wellbore buildup temperatures. Both figures show wellbore-temperature derivatives for four different gauge locations; $z_g = 0, 50, 100, 500$ m for a case where skin is zero (Case 1 of Table 2). Clearly, as we place our gauge 100 m or more above the sandface, the late-time zero slope line for the drawdown period shifts in the upward direction. This is most likely because of the heat loss parameters on the wellbore temperatures as the fluid rises in the wellbore during drawdown. At this point in time, we do not have an expression for the late-time zero slope line of the wellbore-temperature derivative, though it can be derived by differentiating Eq. 62 and 63. The early-time wellbore temperatures for both drawdown and buildup exhibit a unit-slope line, which may due to the thermal expansion of the fluid in the wellbore. Currently, we do not have an expression of the early-time unit-slope lines exhibited by both drawdown and buildup wellbore temperatures. Clearly, the buildup late-time wellbore temperatures do not contain any reservoir information as the wellbore fluid during buildup cools down to the temperature of the strata across the gauge location as they exponentially decrease as heat losses become steady state. Fig. 12 shows the effect of skin zone on the wellbore temperature derivatives for the constant-rate drawdown period for Case 2 of Table 2 ($r_S = 1.06$ m).

7. NONLINEAR PARAMETER ESTIMATION

We recommend to use the Maximum Likelihood Estimate (MLE) method and the Levenberg-Marquardt algorithm for minimizing the MLE the objective function given by (Kuchuk et al., 2010)

$$O(\mathbf{m}) = \frac{1}{2} I_p N_p \ln\left\{\sum_{i=1}^{N_p}\left[p_{wf,obs,i} - p_{wf,mod,i}(\mathbf{m})\right]^2 + \sum_{i=1}^{N_T}\left[T_{wf,obs,i} - T_{wf,mod,i}(\mathbf{m})\right]^2\right\}, \tag{65}$$

when estimating reservoir and well parameters of interest from transient sandface and wellbore temperature jointly with the pressure data. In Eq. 65, I_p and I_T have values of either 1 or 0 and they are used for matching either pressure data set or temperature data set or both. N_p and N_T are the number of observed pressure data ($p_{wf,obs}$) and observed temperature data $T_{wf,obs}$), respectively. In Eq. 56, **m** represents *M*-dimensional vector of model parameters to be optimized by minimizing Eq. 56. Four the problem of interest here, the unknown model parameter vector can consist of five model parameters:

$$\mathbf{m} = \left[k_O, k_S, r_S, \alpha_t,\ e_{JTW}, \phi\right]^T. \tag{66}$$

Recently, Panini et al. (2019) consider nonlinear parameter estimation based on the MLE from sandface temperature data. They show that the rock, fluid and thermal properties of the skin zone and non-skin zone can be reliably estimated by regressing on temperature transient data jointly with pressure transient data in presence of noise.

8. SUMMARY AND CONCLUSIONS

In this study, we presented semi-analytical and analytical solutions based on a coupled transient wellbore/reservoir thermal model to predict temperature transient measurements made under constant rate and bottom-hole pressure production as well as variable rate and bottom-hole pressure production histories in a vertical or an inclined wellbore across from the producing horizon or at a gauge depth above it. We show that unlike the "sandface" temperature measurements made close to the producing zone, the temperature measurements made at locations significantly above the producing horizon are dependent upon the geothermal gradient and radial heat losses from the wellbore fluid to the formation on the way to gauge and hence more difficult to interpret for well productivity evaluation and reservoir characterization. For the specific example considered in this work, it was found that if the gauge location exceeds 100 m, the wellbore temperatures measured at higher gauge locations from the producing horizon are contaminated by the heat losses to adjacent formation. The solutions can be used as forward models for estimating the parameters of interest by nonlinear regression built on a gradient-based maximum likelihood estimation (MLE) method. Log-log diagnostic and semi-log analysis methods proposed in this study can be used to obtain good initial guesses of parameters which derive the MLE objective function to have reliable optimized estimates. Some applications of this nonlinear parameter estimation will be given in a future study.

REFERENCES

Bircan, D.E.: Modeling and Analysis of Sandface and Wellbore Transient Temperature Data for Liquid-dominated Geothermal Wells in Single Layer Two-Zone Composite Systems. MSc Thesis, in progress, Tulsa University, Tulsa, Oklahoma, USA, (2020).

Abramowitz, M. and Stegun, I.A.: *Handbook of Mathematical Functions with Formulas, Graphs, and Mathematical Tables*, Tenth Editing, U.S. Department of Commerce, National Bureau of Standards, Washington (1972), 229.

Alves, I. N., Alhanati, F. J. S., and Shoham, O.: A Unified Model for Predicting Flowing Temperature Distribution in Wellbores and Pipelines. *SPE Prod Eng* 7 (4), (1992), 363-367.

Chekalyuk, E.B., *Thermodynamics of Oil Formation,* (in Russian), Nedra, Moscow (1965).

Chevarunotai N, Hasan A, Kabir C, Islam R (2018) Transient flowing-fluid temperature modeling in reservoirs with large drawdowns. *Journal of Petroleum Exploration and Production Technol*ogy **8**(3): (2018), 799–811.

Curtis, M. R. and Witterholt, E. J.: Use of Temperature Log for Determining Flow Rates in Producing Wells. Presented at the SPE Annual Technical Conference and Exhibition, Las Vegas, Nevada, USA, (1973).

Duru, O.O., and Horne, R.N.: Modelling Reservoir Temperature Transients and Reservoir-Parameter Estimation Constrained to the Model, *SPE Reservoir Evaluation & Engineering*, **13** (6), (2010), 873-883.

Duru, O. O. and Horne, R. N. 2011a. Simultaneous Interpretation of Pressure, Temperature, and Flow-Rate Data Using Bayesian Inversion Methods. *SPE Reservoir Evaluation & Engineering* **14** (2), (2011a), 225-238.

Duru, O.O., and Horne, R.N.: Combined Temperature and Pressure Data Interpretation: Applications to Characterization of Near-Wellbore Reservoir Structures, paper SPE No. 146614, SPE Annual Technical Conference and Exhibition, Denver, Colorado (2011b).

Galvao, M.S.C.: Analytical Models for Thermal Wellbore Effects on Pressure Transient Testing. Master's thesis, PUC-Rio, Rio de Janeiro, Brazil (2018).

Galvao, M.S.C., Carvalho, M.S., and Barreto, Jr. A.B.. A Coupled Transient-Wellbore/Reservoir Temperature Analytical Model. SPE Journal, (2019), preprint: SPE-195592-PA.

Hasan, A. R. and Kabir, C. S. 1994. Aspects of Wellbore Heat Transfer During Two-Phase Flow. *SPE Prod & Fac* 9 (3), (1994), 211-216.

Hasan, A. R., Kabir, C. S. and Wang, X.: Development and Application of a Wellbore/Reservoir Simulator for Testing Oil Wells. *SPE Form Eval* 12 (3), (1997), 182-188.

Hasan, A. R. and Kabir, C. S.: Fluid Flow and Heat Transfer in Wellbores. (2002), SPE, Richardson, Texas, USA.

Hasan, A. R., Kabir, C. S. and Lin, D.: Analytic Wellbore-Temperature Model for Transient Gas-Well Testing. *SPE Res Eval & Eng* 8 (3), (2005), 240-247.

Izgec, B., Kabir, C. S., Zhu, D., and Hasan, A. R.: Transient Fluid and Heat Flow Modeling in Coupled Wellbore/Reservoir Systems, SPE Res Eval & Eng 10 (3), (2007), 294-301.

Kuchuk FJ, Onur M, Hollaender F.: *Pressure transient formation and well testing: convolution, deconvolution and nonlinear estimation*, vol 57. (2010), Elsevier.

Kutun, K, Tureyen, O.I, and Satman, A.: Temperature Behavior of Geothermal Wells During Production, Injection and Shut-in Operations, *Proceedings*, 39th Workshop on Geothermal Reservoir Engineering, Stanford University, Stanford, CA (2014).

MacDonald, R. C. and Coats, K. H.: Methods for Numerical Simulation of Water and Gas Coning. Society of Petroleum Engineers Journal, 10(04), (1970), 425-436.

Mao Y, Zeidouni M, et al.: Accounting for Fluid-Property Variations in Temperature Transient Analysis. *SPE Journal* 23(03), (2018), 868–884.

Miller, C. W.: Wellbore Storage Effects in Geothermal Wells. *SPE Journal* 20 (2), (1980), 555-566.

Moore W.J.: Physical Chemistry. Prentice Hall, Englewood Cliffs: New Jersey (1972).

Onur, M and Palabiyik, Y.: Nonlinear Parameter Estimation Based on History Matching of Temperature Measurements for Single-Phase Liquid-Water Geothermal Reservoirs, *Proceedings*, World Geothermal Congress, Melbourne, Australia, (2015).

Onur, M., Palabiyik, Y., Tureyen, O.I., Cinar, M. Transient temperature behavior and analysis of single-phase liquid-water geothermal reservoirs during drawdown and buildup tests: Part II. Interpretation and analysis methodology with applications, *Journal of Petroleum Science and Engineering* 146, (2016), 657-669.

Onur M, and Cinar M.: Analysis of Sandface-Temperature-Transient Data for Slightly Compressible, Single-Phase Reservoirs. *SPE Journal* 22(04), (2017a), 1134-1155.

Onur M, and Cinar M.: Modeling and Analysis of Temperature Transient Sandface and Wellbore Temperature Data from Variable Rate Well Test Data. In *proceedings* of SPE Europec featured at 79th EAGE Conference and Exhibition, Paris, France, 12-15 June (2017b).

Onur, M., Ulker, G., Kocak, S, and Gok, I.M. Interpretation and Analysis of Transient Sandface and Wellbore Temperature Data. *SPE Journal* 22(04), (2017), 1156-1177.

Onur, M. and Ozdogan, T.: Analysis of Sandface Temperature Transient Data Under Specified Rate or Bottomhole Pressure Production from a No-Flow Composite Radial Reservoir System. In: Paper SPE 195548 presented at SPE Europec featured at 81st EAGE Conference and Exhibition, London, UK, 3 - 6 June (2019).

Onur, M., Galvao, M., Bircan, D.E., Carvalho, M., and Abelardo, B.: Analytical Models for Interpretation and Analysis of Transient and Wellbore Temperature Data. In: Paper SPE 195991 presented at SPE Annual Technical Conference & Exhibition, Calgary, Alberta, Canada, 30 September – 2 October (2019).

Palabiyik, Y., Tureyen, O.I., Onur, M., and Deniz, M.: A Study on Pressure and Temperature Behaviors of Geothermal Wells in Single-Phase Liquid Reservoirs, *Proceedings*, 38th Workshop on Geothermal Reservoir Engineering, Stanford University, Stanford, CA (2013).

Palabiyik, Y., Tureyen, O.I., and Onur, M.: Pressure and Temperature Behaviors of Single-Phase Liquid Water Geothermal Reservoirs Under Various Production/Injection Schemes, *Proceedings*, World Geothermal Congress, Melbourne, Australia, (2015).

Palabiyik, Y., Onur, M., Tureyen, O.I., Cinar, M. Transient temperature behavior and analysis of single-phase liquid-water geothermal reservoirs during drawdown and buildup tests: Part I. Theory, new analytical and approximate solutions, *Journal of Petroleum Science and Engineering* 146, (2016), 637-656.

Panini, F., Onur, M. and Viberti, D.: An Analytical Solution and Nonlinear Regression Analysis for Sandface Temperature Transient Data in the Presence of a Near-Wellbore Damaged Zone. *Transport Porous Media,* (2019), preprint, https://doi.org/10.1007/s11242-019-01306-x.

Ramazanov, A. Sh. and Nagimov, V. M.: Analytical Model for the Calculation of Temperature Distribution in the Oil Reservoir during Unsteady Fluid Flow. Oil and Gas Business, 1/2007 (17.05.07): (2007) 532.546-3:536.42.

Ramey, H. J. Jr.: Wellbore Heat Transmission. *J Pet Technol* 14 (4), (1962), 427-435.

Sagar, R., Doty, D. R., and Schmidt, Z. Predicting Temperature Profiles in a Flowing Well. *SPE Prod Eng* 6 (4), (1991), 441-448.

Sidorova, M., Shako V., Pimenov V. et al.: The value of transient temperature responses in testing operations. Presented at the SPE Middle East Oil & Gas Show and Conference, Manama, Bahrain, (2015).

Stehfest, H.: Algorithm 368: Numerical Inversion of Laplace Transforms. Comm. ACM 13 (1), (1970), 47-49.

Sui, W., Zhu, D., Hill, A.D., and Ehlig-Economides, C.: Model for Transient Temperature and Pressure Behavior in Commingled Vertical Wells, SPE Russian Oil and Gas Technical Conference and Exhibition, Moscow (2008a).

Sui, W., Zhu, D., Hill, A.D., and Ehlig-Economides, C.: Determining Multilayer Formation Properties from Transient Temperature and Pressure Measurements, paper SPE No. 116270, SPE Annual Technical Conference and Exhibition, Denver, Colorado (2008b).